Modeling the microstructure of a heterogeneous particle-based material with high-volume fraction

Ghazal Afshar [a], Adrien Couture [a], Jean-Christophe Cuillière [a*], Vincent François [a]

[a] *ERICCA, Université du Québec à Trois-Rivières (UQTR), Trois Rivières, Québec, Canada*

Abstract

Efficiently predicting the mechanical properties of particle-based heterogeneous materials in terms of both time and cost remains a significant research challenge. This paper introduces two distinct approaches to modify an existing method for the automatic generation of statistical volume elements (SVEs) based on multibody dynamics. These modifications aim at enhancing the accuracy of modeling SVEs with high particle volume fractions, particularly for complex particle shapes. By refining the SVE generation process, the two proposed approaches address challenges in particle positioning and meshing, ultimately contributing to more reliable predictions of materials macroscopic behavior. The first approach involves slightly adjusting the geometric parameters of particles to increase the number of particles that can be inserted and retained within the SVE. The second approach involves generating a larger domain with a target volume fraction, meshing the entire model of this larger domain, and subsequently cutting its mesh to achieve the SVE desired dimensions and to minimize boundary effects. Both approaches are applied to SVEs filled with spherical and cylindrical particles to achieve target volume fractions up to 30%. Results obtained with these two approaches are then compared to those obtained using the existing method. The findings indicate that the geometry correction approach effectively increases the volume fraction of SVEs containing spherical particles, while the mesh cutting approach successfully raises, to the target level, the volume fraction of SVEs containing even more complex elongated particles like cylindrical particles.

Keywords: Finite Element Analysis, Multibody Dynamics, Representative Volume Element, Statistical Volume Element, Geometry Correction Method, Mesh Cutting Method, Particle-based Composites, Homogenization

1. Introduction

The evolution from metal and ceramic materials to synthetic fiber-reinforced composites, and eventually to natural fiber-reinforced polymer composites (NFRPC), reflects the continuous effort to obtain new material characteristics that can better fulfill the demands of various industries [1-3]. Accurately estimating the effective properties of a composite material is crucial for its efficient and precise selection. Evaluating the elastic properties of heterogeneous materials through experimental tests is often time consuming and cost inefficient. Instead, analytical and numerical modeling techniques are available, with microstructural modeling using finite element analysis (FEA) combined with homogenization being one of the most commonly used and accurate methods for estimating the effective properties of heterogeneous materials [4-6]. This combined approach improves the accuracy of simulations and aids in the design and optimization of advanced materials. Homogenization is a method used to determine the effective properties of a composite materials by averaging its microstructural characteristics. FEA simulates the detailed interactions within the microstructure, while homogenization generalizes FEA results to predict macroscopic properties, such as the effective elastic modulus and thermal conductivity. Although the combination of FEA and homogenization provides detailed insights into material behavior, it also presents challenges, such as its high computational costs and the requirement for precise microstructural data. As more details are incorporated into the model, its complexity increases, leading to higher computational time and cost. Therefore, careful consideration is required to balance detail and efficiency in modeling efforts.

In numerical homogenization, the material's response is computed using numerical methods like FEA on a representative volume element (RVE), which is a key concept in numerical homogenization. One of the challenges with RVE based approaches is ensuring that the selected volume accurately represents the entire material. The first step in numerical homogenization is determining the size of the RVE, for which several methods have been proposed [7-9]. It has been demonstrated in [10] that making a direct relationship between a RVE and the material microstructure is not always possible. In certain cases, such as with materials like cement or wood, the shape, size, or heterogeneities of the material microstructure may result in a RVE that is too large for calculations. To address this issue, multiple smaller volumes, referred to as Statistical Volume Elements (SVEs), can be used, with material properties being calculated by averaging over these smaller volumes. In this context, a crucial step is generating volume elements that

statistically approximate the real material's microstructure as closely as possible, which remains a subject of extensive research. In this direction, to ensure that a generation method is both general and effective, several factors must be considered, among which geometry of fibers, their distribution, orientation, shape, and volume fraction, as these factors significantly influence material properties [11]. Additionally, compatibility with subsequent modeling requirements, such as mesh convergence in FEA, time efficiency, and adaptability to different models are other important considerations.

Numerous studies conducted in [12-14] have addressed various issues and challenges related to generating RVEs and have proposed alternatives aimed at refining and improving RVE generation algorithms to overcome these difficulties. One of these challenges is developing a geometry generation method capable of achieving higher fiber volume fractions, which is particularly crucial for particle-based composites. Research has shown that effective material properties are largely influenced by the fiber volume fraction [15]. Indeed, studies have demonstrated that higher fiber aspect ratios or increased fiber volume fractions correlate with enhanced effective properties of materials [16]. Therefore, it is crucial to design generation algorithms capable of producing relatively high-volume fraction of particles, particularly when working with materials featuring high volume fractions, to avoid underestimating their effective properties.

A widely used geometry generation method is random sequential adsorption (RSA). Although this method has been employed by many researchers, it is limited to an inclusion volume fraction known as the jamming limit [17, 18]. Essentially, this means that once a specific volume fraction is reached, where the space between inclusions becomes smaller than the size of inclusions, adding more inclusions is no longer possible. This happens because, with the classical RSA algorithm, once inserted, each accepted inclusion cannot move or be modified to make space for additional inclusions.

Several modifications to the classical RSA have been proposed to achieve higher volume fractions. Kari et al. [19] suggest that once the jamming limit is reached with several fibers of a specific aspect ratio, fibers with lower aspect ratios can be introduced into the cube. This process can be repeated while ensuring that the newly introduced fibers are not too small. They report that this modified RSA approach enables achieving higher volume fractions than with previous versions of the RSA algorithm. Tian et al. [20] introduce a fiber growth method that builds on the

principles of RSA but utilizes a different approach for fiber insertion. Instead of inserting a fiber and checking for intersections with other fibers, the inserted fiber grows from zero length until it intersects with existing fibers.

Rigid Multibody Dynamics (MBD) is another geometry generation method that can be used to overcome RSA limitations. This approach is based on letting the inclusions move and collide with each other. This approach is generally categorized into two groups, referred to as event-driven and time-driven approaches [21]. Event-driven algorithms calculate the next event at a specific moment, such as the collision between two particles or between one particle and boundaries of the domain, after which the state of the system is updated. This includes determining the new position of each particle, its speed, angular velocity, mass and its orientation in the case of a non-spherical particle. Consequently, the system's state is not computed at regular time intervals; instead, the duration of time steps is adjusted according to time intervals between each event. Lobachevsky et al. [22, 23] propose an event-driven method based on Molecular Dynamics (MD) and apply it to discs and spheres. The initial state is established by randomly generating the positions of N points (representing the centers of all particles) within a closed domain. Each point is assigned an initial velocity vector, with its components also drawn randomly. Initially, these points represent spheres with a zero diameter. As each particle moves according to its initial velocity vector, its diameters increase over time. Along this movement and growth, the particles collide elastically. This algorithm requires calculating the positions and velocities of particles at each time step, as well as predicting future collisions. The growth of spheres allows increasing the volume fraction of particles over time, and the process stops once the desired volume fraction is achieved. Li et al. [24] developed an algorithm based on the event-driven MD theory to rapidly generate periodic RVEs with nonuniform distributions for both unidirectional fibre-reinforced and spherical particle-reinforced composites. In [25], a novel algorithm referred to as the sequential adsorption algorithm is introduced for generating RVEs of composites reinforced with randomly distributed spherical particles. This method combines the RSA algorithm with the MD-based approach. The proposed algorithm addresses limitations of the RSA method and can efficiently produce RVEs with high particle volume fractions (around 50%). Despite the developments mentioned above, event-driven MD-based methods are constrained by their limitations regarding collision detection, which restricts all these approaches to spherical particles. Achieving high volume fractions of particles with more complex shapes, such as cylindrical particles, particularly those with high aspect ratios, remains a significant challenge.

In contrast, time-driven MBD approaches calculate the system's state at regular time intervals, updating collision detection at each step. This method is not constrained to specific particle shapes and employs surface triangulations along with bounding boxes for effective collision detection. This approach, employed by our research team (ERICCA) and presented in [26], is used for modeling and analyzing particle-based composites with spherical and cylindrical shapes. The developed method automatically generates the geometry of SVEs using time-driven rigid MBD techniques in conjunction with solid modeling concepts. To ensure that mesh elements show acceptable quality and lead to sufficiently accurate FEA results, specific criteria regarding minimum distance and minimum angle between geometric entities must be adhered to along the generation of particles. This requirement results in the elimination of a significant number of particles, particularly those located near boundaries of the SVE. To address this issue, after FEA results on the entire model are obtained, an erosion of results approach that involves not taking into account results for layers of elements from boundaries of the SVE is integrated into the method. This erosion of results approach, reviewed in section 2, is applied to both the RSA method and the MBD method [26, 27], achieving a volume fraction of approximately 30% for both spherical and cylindrical particles. In this erosion of results approach, to reach the target volume fraction, results inside a distance from the six faces of the SVE, referred to as the erosion distance (d_e) are eroded. This results in a smaller homogenization domain if compared to the original SVE used for FEA. While this approach addresses the issue of inhomogeneity near the boundaries, it raises important questions about the exclusion of boundary elements results. Specifically, it is necessary to determine whether a high volume fraction with a uniform particle distribution can be achieved without removing these boundary elements results or encountering inhomogeneity at the SVE boundaries.

In the present work, the objective is to generate a number of SVEs that achieves the target volume fraction and can subsequently be submitted to FEA without requiring erosion of results, which means any removal of results. This approach seeks to overcome common issues in modeling, such as lack of particles and voids near SVE boundaries and non-uniform particle distribution, using automated methods based on the MBD generation algorithm. Two distinct strategies are introduced in this paper to achieve higher volume fractions of particles, particularly for cylindrical-shaped particles. Indeed, cylindrical-shaped particles tend to be challenging to model due to their elongated geometry and due to potential particles alignment issues. The first approach proposed is based on integrating a geometry correction process into the MBD algorithm. This approach focuses on ensuring that each particle shape meets geometrical criteria (minimum distance and minimum angle) while minimizing deviations from its original

dimensions. This geometry correction approach is inspired from modifications applied on the RSA algorithm [19, 28], and specifically adapted for its integration into the MBD framework. The main idea is making slight adjustments to particles characteristics, such as size, position, and orientation, while preserving as much as possible the uniform random distribution and isotropic characteristics of the original particles' configuration. The second approach proposed involves using a mesh cutting process. Unlike the geometry correction approach, this method focuses on initially generating a larger domain model and creating a mesh for the entire volume. After generating this mesh, it is cut down to the SVE size, effectively eliminating areas with voids, particularly near the boundaries. This cutting process is particularly useful for elongated particles, such as cylinders, which often lead to voids at the boundary when trying to fit them uniformly within the SVE. This process allows the final SVE to achieve a higher volume fraction and ensures that particles are uniformly distributed across the model without significant boundary effects. The mesh cutting method ensures that the target volume fraction is met without eroding results, which provides a more accurate representation of the material's mechanical behavior under analysis.

The structure of this paper is as follows: Section 2 briefly presents a previous work [26] on the subject, while sections 3 and 4 respectively present the geometry correction and mesh cutting approaches as introduced in the previous paragraph. Section 5 presents results obtained with these two approaches and Section 6 summarizes the main conclusions of this study.

2. A review of the existing Erosion of results Method

This section provides an overview of the erosion of results method applied to MBD, as introduced in [26], providing the necessary background for the new approaches proposed in this work. The foundation for this approach was first established in [27], where a generalized and automated numerical homogenization modeling framework for particle-based heterogeneous materials was developed. This initial work in [27] utilized RSA for geometry generation, providing a structured methodology for simulating particle-based composites. Building on this foundation, the study in [26] retained the same overall framework but introduced the erosion of results method to improve homogenization accuracy. This method was initially applied to models generated using the RSA algorithm. Additionally, to achieve higher particle volume fractions, [26] extended the framework by incorporating the MBD algorithm as an alternative approach to geometry generation, alongside RSA. The erosion of results method was then applied to both RSA and

MBD models to assess its effectiveness. The entire modeling framework of this method is obtained by integrating CAD, mesh generation and FEA tools. This integration is facilitated through the Unified Topology Model (UTM) [29], which establishes a connection between Boundary REPresentation (BREP) topological entities and mesh entities used in FEA. With the UTM, boundary conditions are directly applied to BREP topological entities, and FEA results can be mapped back to the original geometry, allowing for comprehensive post-processing analysis. The main steps of this modeling process include geometry generation, mesh generation, FEA, erosion of results and homogenization of these eroded results to assess effective properties. All these steps are executed automatically and are followed by a post-processing stage, as illustrated in Figure 1. In the first step (Figure 1a), a particle distribution is generated using MBD within a slightly larger domain of length $L + \Delta$, referred to as the MBD generation domain. To ensure mesh convergence in subsequent steps, minimum distance and angle criteria are applied to each particle. Only particles that meet these criteria are inserted into the CAD model of the SVE of length L (Figure 1b). However, the resulting model shows a lack of particles near the boundaries of the sample, leading to a deviation from the target particle volume fraction. Then, the SVE is meshed with quadratic tetrahedral elements (Figure 1c) and FEA is automatically performed (Figure 1d). An erosion of results homogenization method is employed to exclude results for the layers of elements around the boundaries of the SVE (Figure 1e), thereby discarding void regions at these boundaries and improving the accuracy of the macroscopic material behavior obtained at the end of the process.

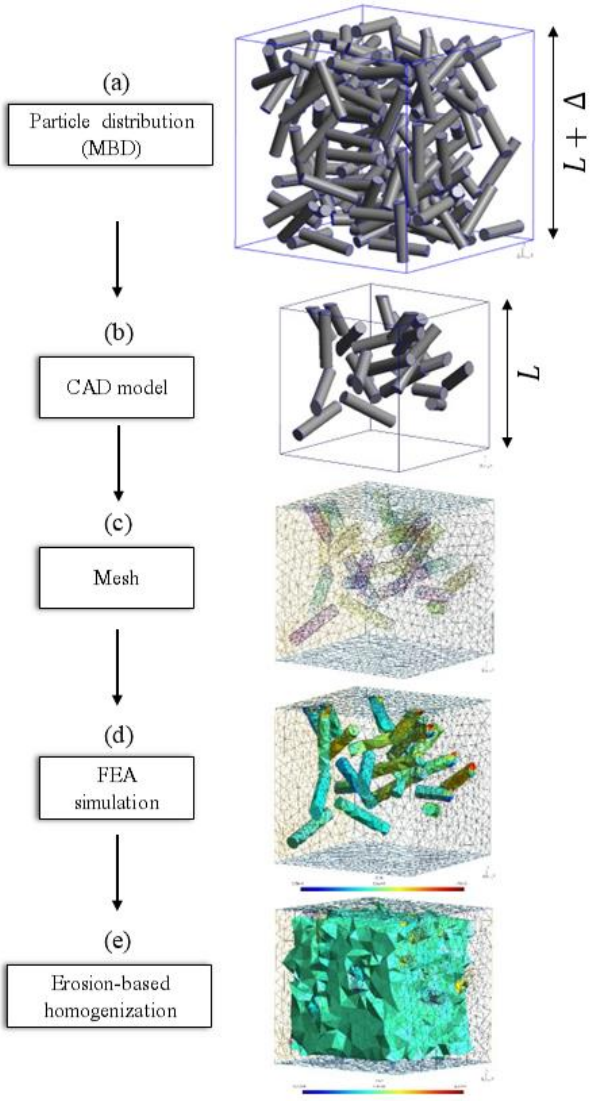

Figure 1. Overview of the SVE automatic generation process described in [26].

As described in the previous section, this method reaches volume fractions up to approximately 30% for both spherical and cylindrical particles. The ability to reach this volume fraction without dealing, through erosion of results, with issues such as lack of particles at SVE boundaries, boundary condition effects, or inhomogeneities, while preserving the FEA results at the boundaries, is addressed by the two approaches presented in the following sections.

3. Geometry Correction Method

In this section, the geometry correction method (GCM) is presented. This work focuses on using MBD to achieve a higher volume fraction without erosion of results. To generate a CAD model of the SVE with a uniform distribution of particles, the first step consists in inserting enough particles to reach the desired volume fraction into a slightly larger domain, referred to as the *MBD generation domain*, without applying intersection criteria. This domain is larger than the SVE ($L + \Delta$) to avoid effects caused by particles in contact with the SVE boundary. Subsequently, the MBD approach is applied using a time-driven algorithm to arrange these particles with the open-source Project Chrono library [30]. During MBD, the dynamics of moving and colliding particles is computed, and a velocity vector is assigned and updated for each particle. Motion and collision equations are iteratively updated at each time step. When convergence of this iterative process is reached, the velocity of each particle is close to zero and the final distribution of particles within the domain is obtained.

Next, the SVE of length L is generated as a CAD model. As introduced earlier, to ensure mesh convergence in subsequent steps, a minimum distance and minimum angle between any two particles, or any particle and the SVE faces, must be maintained. Applying these two geometric criteria might result in the removal of particles, particularly near the SVE boundary, leading to a reduction of the particle volume fraction. To address this issue, an algorithm is introduced to slightly adjust the geometric characteristics of particles that do not meet these two criteria, trying by the way to make these particles compatible. This adjustment enables retaining particles that might otherwise be excluded. Particles that are already compatible with these criteria are directly inserted into the CAD model of the SVE. For each particle that do not meet one (or more) geometric criterion, a process is iteratively applied to slightly adjust its size, position, or orientation. The process begins with a size adjustment phase. During this phase, an adjustment factor ($\propto < 1$) is applied iteratively to gradually reduce the particle's dimensions (length L_P for cylinders or diameter D_P for spheres). At each iteration of size adjustment, the two criteria mentioned above (minimum distance and angle) are re-evaluated. If these criteria are satisfied, the particle is considered compatible and retained in the SVE. If the size adjustment phase alone does not result in compatibility after a maximum number of iterations (it_{max}), the algorithm goes on with a particle position adjustment phase, along which the particle's coordinates $(\mathrm{x}, \mathrm{y}, \mathrm{z})$ are iteratively modified. Like in the size adjustment phase, at each iteration of particle location adjustment, the two criteria are re-evaluated, and compatibility is assessed. For cylindrical particles, if neither size nor position adjustments resolve the

incompatibility, the algorithm ends with an orientation adjustment phase to modify the orientation angles ($\theta\ and\ \varphi$). For each adjustment phase, adjustments are tried iteratively, until a maximum number of iterations (it_{max}) is reached. The primary objective is to retain as many particles as possible without significantly deviating from the original size of its random distribution. The method's algorithm is outlined in Algorithm 1.

Algorithm 1. Geometry correction method

Input: Particles list with properties (size (L_P/D_P), coordinates (x, y, z), type (sphere, cylinder), if cylinder: orientation ($\theta\ and\ \varphi$)),

Output: particles compatible with criteria

Initialization: Initial adjustment factor: $\propto_{initial} < 1$, Maximum number of adjustment iteration: it_{max}, $Create\ particle = False$, i=1, j=1, k=1
Foreach particle, P **do**
  If criteria not satisfied, **then next**
    While $i < it_{max}$ **and** $Create\ particle = False$, **do**
      $\propto_i = \propto_{initial}^{i}$
      In case of cylinder: $L_P = L_P \times \propto_i$
      In case of sphere: $D_P = D_P \times \propto_i$
      If criteria satisfied, **then next**
        $Create\ particle = True$
    If $Create\ particle = False$ **then next**
    While j $< it_{max}$ **and** $Create\ particle = False$, **do**
      $adjust\ x, y, z$
      If criteria satisfied, **then next**
        $Create\ particle = True$
    In case of cylinder:
    If $Create\ particle = False$ **then next**
    While k $< it_{max}$ **and** $Create\ particle = False$, **do**
      In case of cylinder: adjust $\theta\ and\ \varphi$
      If criteria satisfied, **then next**
        $Create\ particle = True$

4. Mesh Cutting Method

This method offers an alternative approach to achieve a uniform particle distribution. Its main objective is eliminating the need for the erosion of results. A stepwise approach is used to reach the SVE of length L (Figure 2). First the MBD generation domain of length L + Δ is defined and all required particles are inserted while ensuring no particle intersections occur (Figure 2a). Then, the CAD model of a smaller domain of length $L + \varepsilon$ while $\varepsilon < \Delta$, referred to as the criteria domain, is created by applying the geometric criteria mentioned in the previous section (minimum distance and minimum angle) to achieve a compatible particle distribution (Figure 2b).

Once this compatible particle distribution is achieved inside the criteria domain, material properties are assigned and the CAD model of this criteria domain is meshed, based on a size map [27]. Quadratic tetrahedral elements with straight edges are automatically generated first. Subsequently, the mesh is trimmed to match the dimensions of the SVE (L), as detailed in Algorithm 2. Tetrahedral elements intersecting the boundary of this SVE are divided into smaller tetrahedra. All elements located outside the SVE are discarded, which results in a mesh of the SVE (Figure 2c). This approach effectively removes boundary areas that are subject to voids and lack of particles, leaving a uniformly and randomly dispersed particle-based SVE cube (Figure 2d).

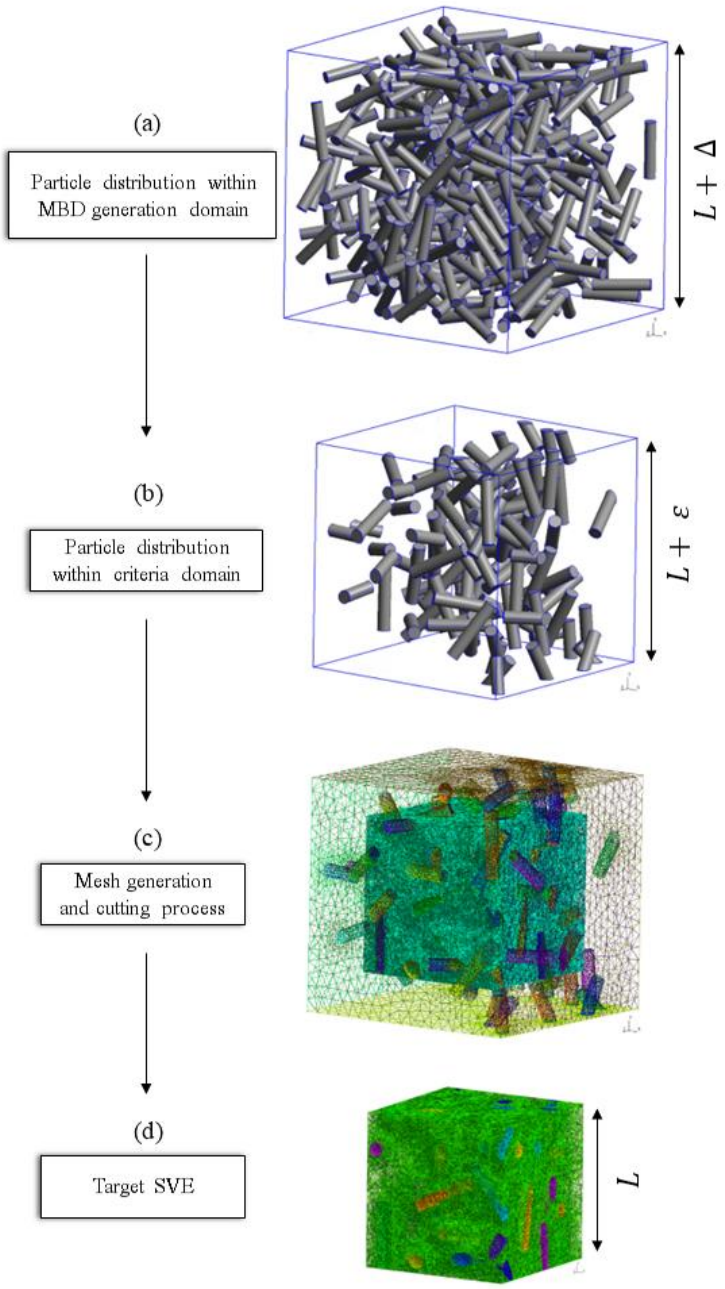

Figure 2. Overview of the SVE automatic generation process with mesh cutting method ($\varepsilon < \Delta$).

The algorithm for cutting the mesh by the six planes of the SVE boundary is presented as Algorithm 2. The entire process involves four loops. The first loop iterates over the six cutting planes of the SVE cube and the next three inner loops respectively iterate over all nodes, segments, and tetrahedral elements in the mesh. For each cutting plane, the process begins with a loop over all nodes that first calculates the distance between each node and the cutting plane

($dist_{node\_n}$). There are three possible states for each node with respect to a given cutting plane: inside the SVE (represented by a positive distance, +), outside the SVE (represented by a negative distance, -), or on the plane (represented by zero distance, 0). Using this information, the next loop checks mesh segments and creates a list of segments being intersected by the plane ($list_{cut\_seg}$). Segments with one node inside ($dist_{node\_n} > 0$) and the other outside ($dist_{node\_n+1} < 0$) are added to this list. For each mesh segment in this list, the coordinates of the intersection between the segment and the plane are calculated, resulting in a point. A new node is created at these coordinates and assigned to its respective segment. Then, the algorithm iterates over each tetrahedral element to assess the state of its four nodes. These iterations result in all tetrahedrons being classified as inside, outside, or cut by the cutting plane. All tetrahedrons located outside the SVE are removed from the mesh, while all tetrahedrons located inside the cube are retained unchanged. The classification of all possible ways of leading to an inside or outside tetrahedron, based on the state of its four nodes, is shown in Table 1. For tetrahedrons intersecting the cutting plane, six different cutting scenarios are shown in Figure 3. For each tetrahedron being cut, a list of nodes is created including inside nodes, on plane nodes, and newly created nodes at intersections with the cutting plane. Based on the number and type of nodes inside this list, the inside part of each cut tetrahedron could result in a tetrahedron itself (list of four nodes), a quadrilateral pyramid (list of five nodes) or a triangular prism (list of six nodes). This classification of cutting scenarios is summarized in Table 2.

Algorithm 2. Mesh cutting process.

Input: Mesh file, six cutting planes coordinates,
Output: Mesh file of cut mesh

Foreach cutting plane, $Plane_i$ (i=1 to 6)
  Foreach node **do**
    Get node distance from $Plane_i$, $dist_{node\ n}$
  Foreach segment **do**
    Get two nodes of segment ($node_n$, $node_{n+1}$) and their distances from cutting plane $dist_{node\ n}$, $dist_{node\ n+1}$
    If ($dist_{node\ n}$ >0 and $dist_{node\ n+1}$ <0) **or** ($dist_{node\ n+1}$ >0 and $dist_{node\ n}$ <0)
      Calculate segment and $Plane_i$ intersection coordinates, x, y, z
      Create a node in x, y, z and attach it to segment, $new\_node_{segment}$
  Foreach tetrahedral element, tetra **do**
    Get four nodes of tetra distance from $Plane_i$,
    If all four $dist_{node}$ are <=0 **then next**
      Remove tetra
    Else if all four $dist_{node}$ are >=0 **then next**
      Keep tetra
    Else
      Generate a list of nodes, $List_{nodes}$
      Insert nodes with $dist_{node}$ >=0
      Insert $new\_node_{segment}$ attached to tetra's segments
      Get number of nodes inside $List_{nodes}$, No_{nodes}
      If No_{nodes} = 4 **then next**
        Generate a new tetra element by these nodes
      If No_{nodes} = 5 **then next**
        Generate two new tetra elements by these nodes
      If No_{nodes} = 6 **then next**
        Generate three new tetra elements by these nodes

Table 1. Various configurations of a tetrahedron before cut based on the states of its four nodes.

Tetrahedron node number	1	+	+	+	+	−	−	−	−
	2	+	+	+	0	0	−	−	−
	3	+	+	0	0	0	0	−	−
	4	+	0	0	0	0	0	0	−
Tetrahedron state		Inside	Inside	Inside	Inside	Outside	Outside	Outside	Outside

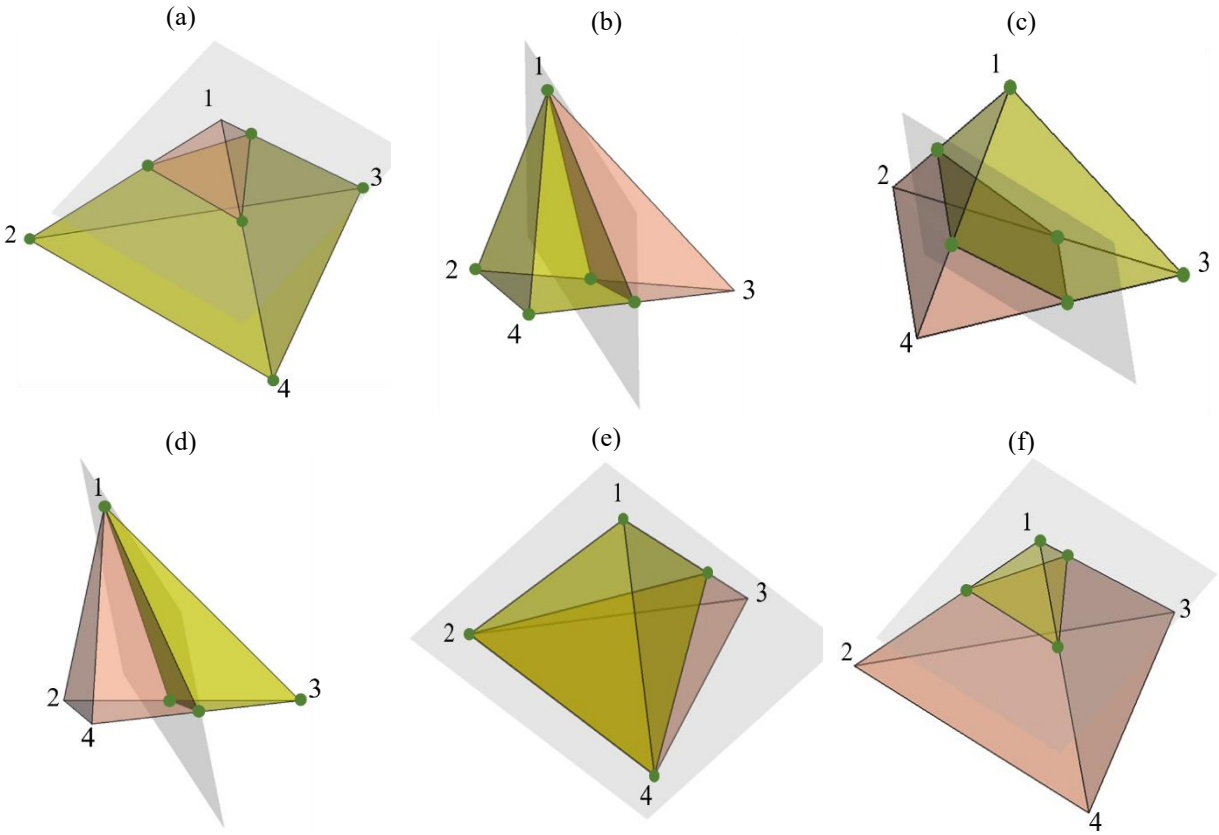

Figure 3. Six different configurations of a cut tetrahedron based on the state of its four nodes, yellow is the inside part of the tetrahedral element, red is the outside part of the tetrahedral element, and the final inside nodes and newly created nodes on segment and cutting plane intersection are shown in green.

Table 2. Six different configurations of a cut tetrahedron determined by the state of its four nodes: "+" (inner side of the cutting plane), "-" (outer side of the cutting plane), and "0" (on the cutting plane).

Tetrahedron state		Cut tetrahedron (a)	Cut tetrahedron (b)	Cut tetrahedron (c)	Cut tetrahedron (d)	Cut tetrahedron (e)	Cut tetrahedron (f)
Tetrahedron nodes	1	+	+	+	+	+	+
	2	+	+	+	0	0	−
	3	+	0	−	−	0	−
	4	−	−	−	−	−	−
final number of nodes inside the list		6	5	6	4	4	4
final shape of inside part		triangular prism	quadrilateral pyramid	triangular prism	tetrahedron	tetrahedron	tetrahedron

When the resulting list of nodes contains four nodes, arranging them in the correct order is sufficient to form a properly oriented tetrahedral element. However, when the list contains five or six nodes, additional considerations are required. A quadrilateral pyramid can be divided into two tetrahedra by splitting its quadrilateral face (Figure 4), while a triangular prism can be divided into three tetrahedra by splitting each of its three quadrilateral faces (Figure 5). Since a quadrilateral pyramid must be divided into two tetrahedra, splitting the quadrilateral face requires consideration of neighboring tetrahedra to ensure mesh consistency. There are two possible ways to split a quadrilateral face into two triangles, and the appropriate splitting diagonal must be chosen based on the configuration of neighboring elements to maintain consistency and quality of the resulting mesh. This issue also applies to splitting a triangular prism since there are three quadrilateral faces to split.

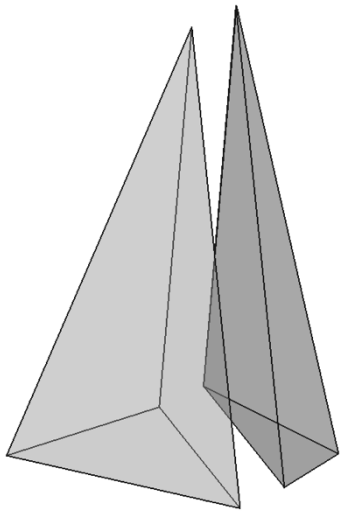

Figure 4. A quadrilateral pyramid being tessellated into two tetrahedra.

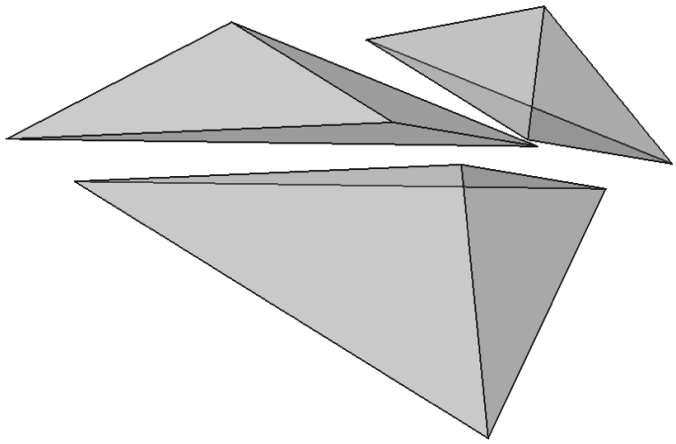

Figure 5. a triangular prism being tessellated into three tetrahedra.

Indeed, there are eight different ways to create diagonals and split the three quadrilateral faces of a triangular prism. However, only configurations for which two of the three diagonals coincide in one of the prism corners are valid and result in three tetrahedra. Thus, as reported in [31-33], there are six ways to create three tetrahedra from a triangular prism (Figure 6). The choice of how the three quadrilateral faces is divided is important since neighboring tetrahedra should also be considered to guarantee mesh consistency. In the mesh generation algorithm, each node is associated with the triangles it belongs to. Using this information, the algorithm evaluates all six possible ways to create tetrahedra from a triangular prism and selects the one that fits with the existing triangles formed by any three of the six nodes. Another challenge is related to cases when the process leads to a dead-end because it reaches a triangular prism for which all three quadrilateral faces are already divided consistently with its neighboring tetrahedra in way that is not valid (not consistent with the six configurations shown in Figure 6). These dead-end cases are addressed by creating a new node inside the prism and eight tetrahedra are generated inside the prism with the help of this new node (Figure 7). In this work, across the entire model, dead-end scenarios usually occur for less than 0.2% of all tetrahedra being cut. Maintaining this percentage as low as possible is important because a higher percentage would lead to increasing the number of nodes and elements being created, which in turn raises computational time.

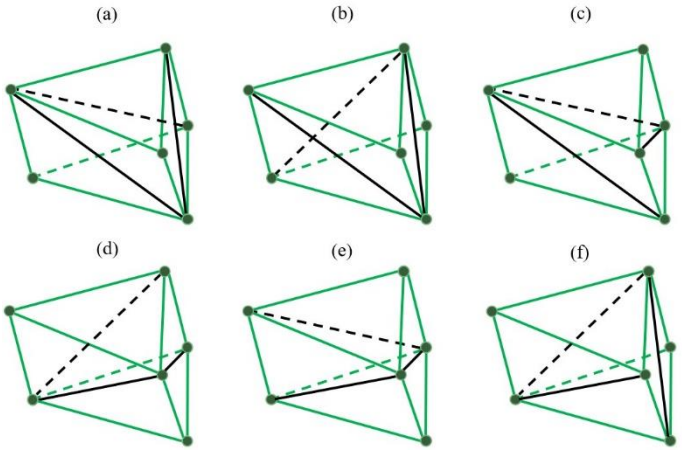

Figure 6. Six valid different ways to create three tetrahedra from a triangular prism.

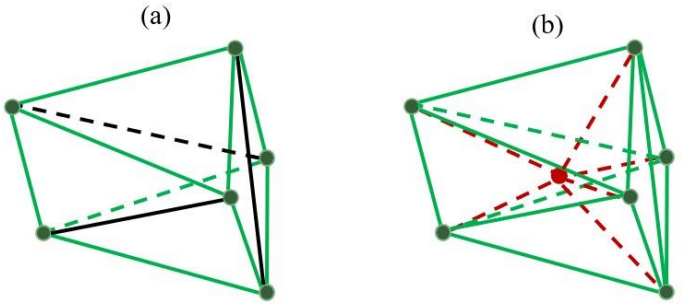

Figure 7. Addressing the dead-end problem in a triangular prism by adding a new node inside it.

A schematic of the cutting process is illustrated in Figure 8. The new mesh exhibits poor quality around the SVE faces due to the cutting process, which is improved through a mesh optimization step. It must be underlined that during the cutting process, the link between the CAD model (BREP topology) and mesh components (nodes, triangles, tetrahedra) is lost since some particle geometries are removed and new mesh elements are generated. As a result, original connections between CAD and mesh components are lost. As the UTM workflow requires an associated geometric model, a virtual CAD geometry of the SVE is defined, since no geometric model initially exists for it. This virtual geometry is constructed by associating topological entities (such as edges, faces, and volumes) with geometric entities that are derived from the mesh. These geometric entities are implicitly defined using information of elements that are cut into new elements during the cutting process. In other words, the mesh itself, combined with its transformation, serves as a foundation to recreate a geometric structure indirectly. This virtual CAD geometry is not

an actual representation of the original geometry but serves as an approximation, allowing the re-establishment of links between geometry and mesh, in order to apply boundary conditions and material properties.

It is also worth noting that curvilinear quadratic tetrahedra are generated based on linear tetrahedra. Without knowledge of the actual geometry, this quadratization is carried out by pushing nodes onto an approximated geometry of particles faces, which is based on the calculation of the local discrete curvature [34]. Once mesh optimization and quadratization completed, applying boundary conditions, FEA and homogenization of results are automatically performed. This method eliminates areas located around faces of the cut criteria domain with lower particle density, leading to a more uniform particle distribution inside the SVE itself.

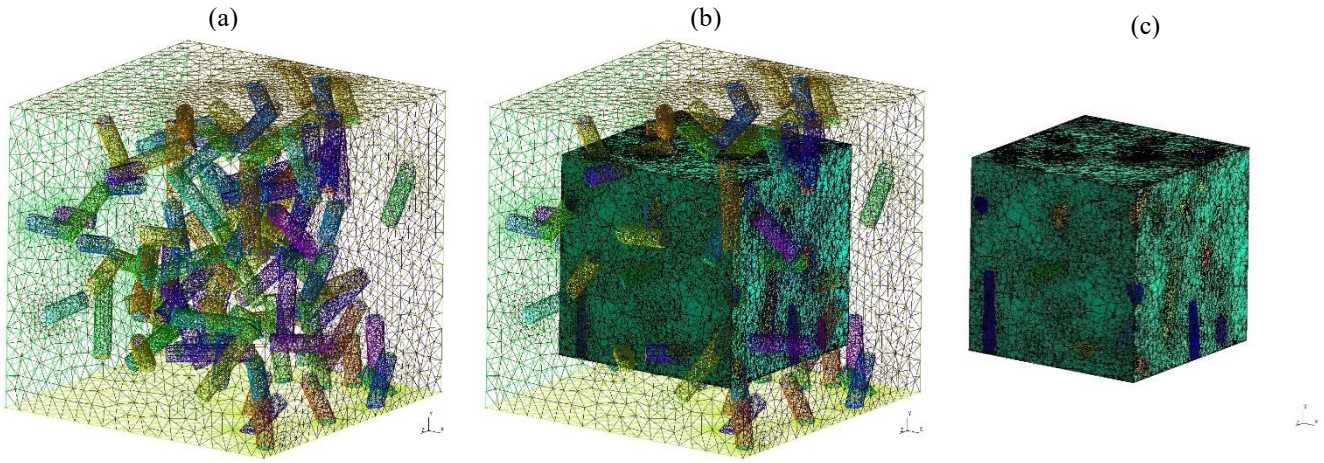

Figure 8. (a) meshed criteria domain, (b) cut criteria domain by target SVE and generation of new elements (the target SVE is shown by 3D elements and outer criteria domain by 2D elements for clarification.), (c) removal of outside tetrahedra leading to the target SVE.

5. Results and discussion

To illustrate the advantages of the two improvement methods detailed previously, this section presents results obtained using the geometry correction and mesh cutting methods. It must be reminded that the primary goal of these two methods is raising the volume fraction of particles inside a SVE while maintaining an isotropic distribution of these particles.

5.1. Results obtained with the geometry correction method

This section presents results obtained for SVEs with unit cube dimensions ($L = 1$) using the GCM. Two types of particle shapes, spherical and cylindrical, are considered. The geometric specifications of spherical and cylindrical particles used are detailed in Table 3.

Table 3. Particle characterization used in modeling.

Particle	Label	Particles intersecting the SVEs borders	Geometrical properties	volume fraction (%)	Number of samples
sphere	S1	Yes	$D = \frac{1}{6}$	10	15
	S2	Yes	$D = \frac{1}{6}$	30	15
cylinder	C1	Yes	$D = 0.085, \frac{L}{D} = 5$	10	15
	C2	Yes	$D = 0.085, \frac{L}{D} = 5$	30	15

For each particle shape, two target volume fractions are considered: 10% and 30%. As detailed earlier, using the MBD algorithm, particles required to achieve the target volume fraction, are inserted into the MBD generation domain. Geometric criteria (minimum distance and minimum angle) are then applied to all particles, and they are free to intersect with the SVEs borders. The final distribution of particles that comply with these criteria is displayed in Figure 9a (10% target volume fraction) and Figure 9d (30% target volume fraction) for spherical particles and Figure 10a (10% target volume fraction) and Figure 10d (30% target volume fraction) for cylindrical particles. Any particle that does not meet one of the two geometric criteria undergo the geometry correction algorithm. The final distribution of particles that have been modified in shape, position, or orientation to ensure compatibility with the two geometric criteria, is illustrated in Figure 9b (10% target volume fraction) and Figure 9e (30% target volume fraction) for spherical particles and Figure 10b (10% target volume fraction) and Figure 10e (30% target volume fraction) for cylindrical particles. The inclusion of these newly retained particles, along with those already accepted and inserted, results in the final particle distribution and volume fraction, as illustrated in Figure 9c (10% target volume fraction) and Figure 9f (30% target volume fraction) for spherical particles, and Figure 10c (10% target volume fraction) and Figure 10f (30% target volume fraction) for cylindrical particles.

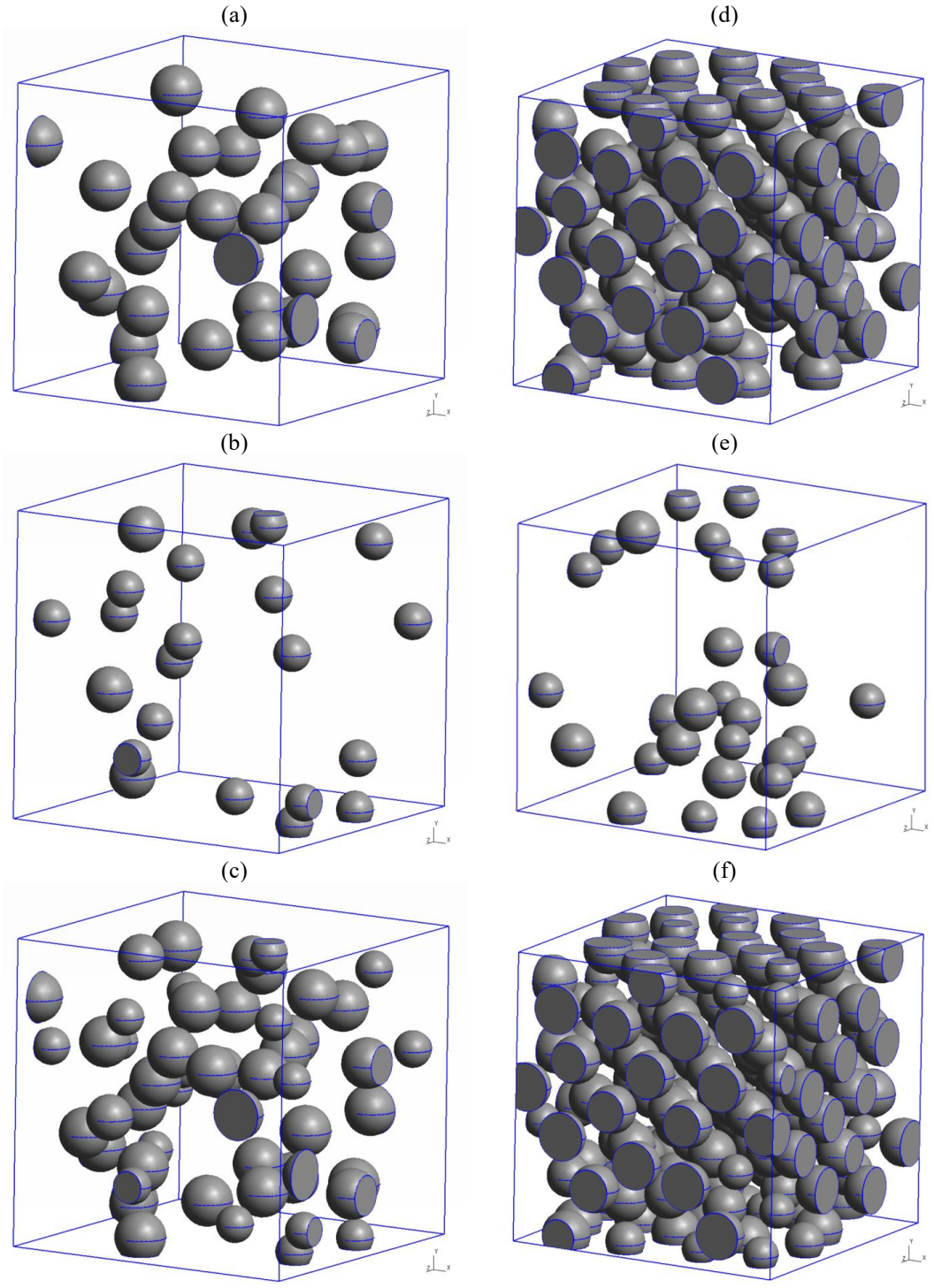

Figure 9. Geometry correction approach for spherical particles to achieve 10% volume fraction ((a)-(c)) and 30% volume fraction ((d)-(f)). Shown are original particle distribution ((a), (d)), corrected and accepted particles ((b), (e)), and final particle distribution ((c), (f)).

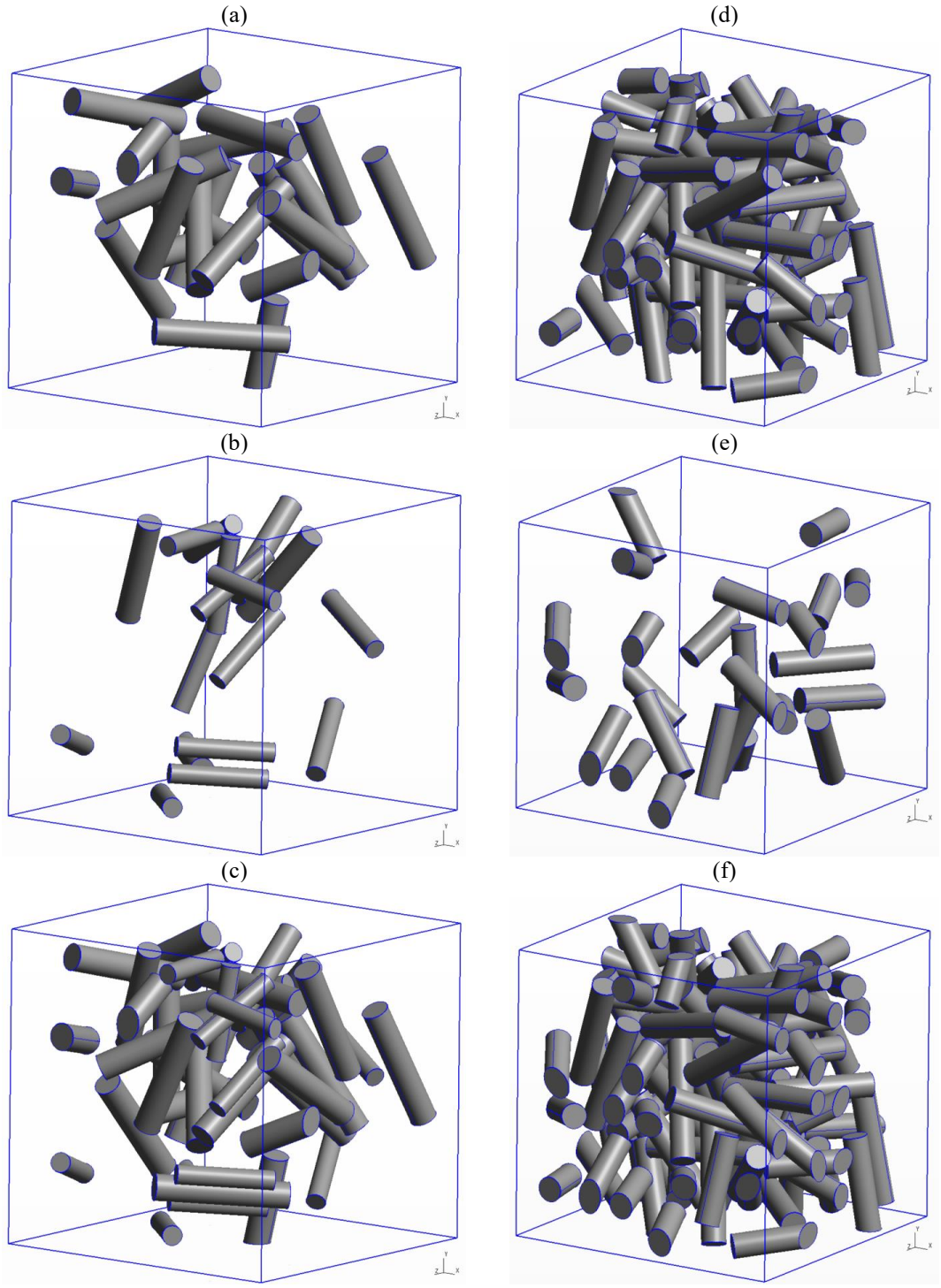

Figure 10. Geometry correction approach for cylindrical particles to achieve 10% volume fraction ((a)-(c)) and 30% volume fraction ((d)-(f)). Shown are original particle distribution ((a), (d)), corrected and accepted particles ((b), (e)), and final particle distribution ((c), (f)).

Numerical results, including the mean volume fraction and mean number of particles of 15 SVEs for each case, are summarized in Table 4. For spherical particles, before applying the GCM, mean volume fractions around 7.17% and 27.60% are respectively obtained for 10% and 30% target volume fractions. After applying the geometry correction algorithm, these mean values increase to 9.62% and 30.63%. Changes to the geometry in this case are limited to changing the radius and position of spheres, which is significantly different for cylindrical-shaped particles. When the GCM is not applied, with cylindrical particles, mean volume fractions around 4.78% and 15.31% are respectively obtained for 10% and 30% target volume fractions. After applying the geometry correction algorithm, these mean values increase to 7.41% and 19.75%. For cylindrical particles, the algorithm tries adjustments in length, radius, position, and orientation of particles. Even if this approach enhances the volume fraction, it still falls short of achieving target volume fractions for elongated particles. This limitation arises because, although several particles are retained, their volume is often significantly reduced. Moreover, after a limited number of adjustments, a jamming limit is reached. As a particle's position or orientation is modified to resolve a compatibility issue with one neighboring particle, it can create a new compatibility problem with another neighboring particle. For instance, in Figure 11, even after adjusting the position of particle 2 to ensure it respects the minimum distance between the particle and the SVE boundary, a new incompatibility arises with particle 1. As a result, particle 2 is ultimately removed from the SVE model. Furthermore, when working with cylindrical particles, ensuring a final isotropic distribution necessitates careful attention to their random positioning and orientation which is checked using the orientation tensor of particles. When the correction algorithm modifies orientation and position of cylinders to achieve a higher volume fraction, it may disrupt the random distribution of particles' orientation. This issue is illustrated in Figure 12. The figure illustrates that the correction algorithm may tend to align particles that were randomly oriented before geometry correction, which ultimately results in a non-isotropic distribution of particles orientation. The alignment shown in Figure 12b is measured using the orientation tensor illustrated in Table 5. Indeed, the diagonal values of this tensor exhibit deviations (around 10%) from those in the tensor of a perfectly isotropic distribution of particles.

To achieve a higher volume fraction for more complex shapes than spheres, which is generally the case for real-world particle geometries, the mesh cutting method can be applied. The results of this method are presented in the next subsection.

Table 4. Results of applying GCM on SVEs.

Case	Target volume fraction (%)	MBD without GCM (%)	MBD with GCM (%)	Number of Corrected Particles	Total Number of Particles
S1	10	7.17 ± 0.91	9.62 ± 0.84	19 ± 3	52 ± 5
S2	30	27.60 ± 0.20	30.63 ± 0.30	27 ± 3	162 ± 2
C1	10	4.78 ± 0.50	7.41 ± 0.32	20 ± 3	43 ± 5
C2	30	15.31 ± 0.49	19.75 ± 0.95	31 ± 6	106 ± 2

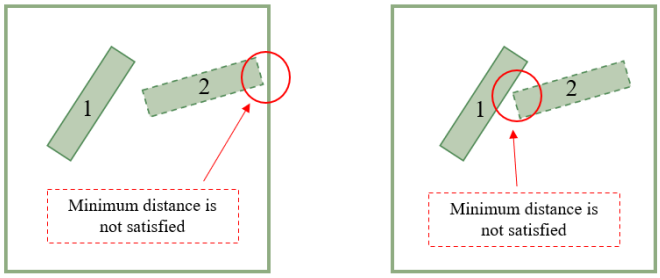

Figure 11. Jamming limit in GCM, $\min_{dist}$ problem of particle 2 (left) with the edge and (right) with another particle.

(a)

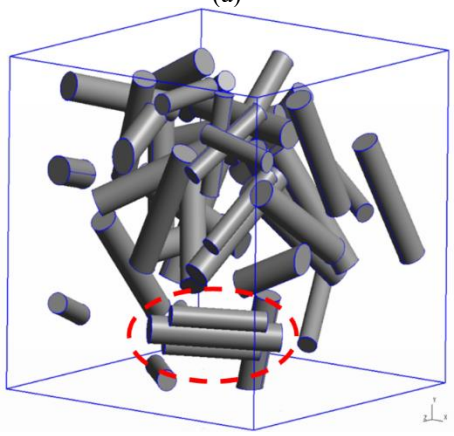

(b)

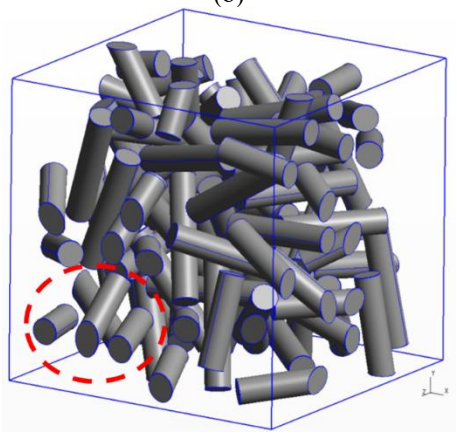

Figure 12. The correction algorithm tends to change the randomly oriented particles to become uniformly aligned, resulting in a non-isotropic distribution of cylinders: (a) for 10% target volume fraction, (b) for 30% target volume fraction.

Table 5. Orientation tensor for sample Figure 12b.

$$\begin{bmatrix} 0.294 \pm 0.039 & -0.023 \pm 0.015 & -0.015 \pm 0.016 \\ -0.023 \pm 0.015 & 0.293 \pm 0.039 & -0.015 \pm 0.018 \\ -0.015 \pm 0.016 & -0.015 \pm 0.018 & 0.411 \pm 0.078 \end{bmatrix}$$

5.2. Results obtained with the mesh cutting method

Following models are generated and evaluated by the mesh cutting method described in section 4. Geometric properties used for these models are listed in Table 6. The results are obtained for SVEs with unit cube dimensions ($L = 1$). Furthermore, material properties of a glass-epoxy composite are used in these models as listed in Table 7.

Table 6. Particle characterization used in modeling.

Particle	Particles intersecting the SVEs borders	Geometrical properties	Volume fraction (%)	Number of samples
Sphere	No	$D = \frac{1}{6}$	30	15
Cylinder	No	$D = 0.085, \frac{L}{D} = 5$	30	15

Table 7. Material properties.

Material	E (GPa)	υ
Epoxy	3.5	0.33
Glass	72.3	0.22

As presented in section 4, the final geometry and mesh of SVEs are generated focusing on mesh consistency and tetrahedral elements quality. As reported in our previous work [26], discarding particles intersecting the borders of SVEs reduces the number of elements and prevents the refinement of the size map near the boundaries. In this method, particles intersecting the borders of the criteria domain are similarly discarded, along with particles that do not meet specified criteria. This approach is justified since elements in these areas will be removed in subsequent steps. The volume fraction is calculated for the criteria domain for comparison purposes, which is followed by mesh generation and mesh cutting to achieve the target SVE dimensions. It is worth noting that the final SVE volume fraction of particles is based on the volume of mesh elements and not on solid modelling calculations. The comparison between these volume fractions is presented in Table 8. Before implementing the mesh cutting method, the maximum achievable volume fractions were 19.34% for spheres and 15.31% for cylindrical particles. It is worth noting that, if compared to spheres, the volume fraction is lower for cylinders due to their geometric characteristics, which make it more challenging to fit a greater number of cylinders inside the SVE while respecting required criteria (minimum distance and angle). However, after applying the mesh cutting method, these values increase to 30.33% for spherical particles and 30.14% for cylindrical particles, which demonstrates the effectiveness of this method towards raising volume fractions.

The orientation tensor for cylindrical particles is presented in Table 9 to verify the isotropic distribution of particles orientation within the SVE. As mentioned in sub-section 5.1, this tensor provides insights into the alignment and distribution of cylindrical particles, ensuring their uniform orientation. This confirms the effectiveness of this method towards achieving isotropic distributions of particles orientation.

Table 8. Comparison of volume fractions with different methods.

	Target volume fraction (%)	Volume fraction in criteria domain (%)	Volume fraction after cut in SVEs (%)	Volume fraction with erosion of results only with erosion of results distance of 0.2 (%) [26]

Sphere	30	19.34 ± 0.34	30.33 ± 0.49	34.12 ± 0.57
Cylinder	30	15.31 ± 0.49	30.14 ± 0.53	27.01 ± 1.88

Table 9. Orientation tensor for cylindrical particles.

$$\begin{bmatrix} 0.323 \pm 0.0244 & -0.004 \pm 0.0240 & -0.003 \pm 0.0283 \\ -0.004 \pm 0.0240 & 0.342 \pm 0.0234 & -0.006 \pm 0.018 \\ -0.003 \pm 0.0283 & -0.006 \pm 0.018 & 0.334 \pm 0.020 \end{bmatrix}$$

The geometric quality of tetrahedral elements in finite element meshes is based on the classical quality metric Q_k, defined as:

$$Q_k = \frac{2\sqrt{6}r}{h_{max}} \tag{1}$$

Where r is the inradius (the radius of the sphere inscribed within the tetrahedron), and h_{max} is the maximum edge length of the tetrahedron. This metric quantifies the element's deviation from the ideal shape, with values ranging from 0 (for a degenerate tetrahedron) to 1 (for a perfect equilateral tetrahedron). Higher values of Q_k indicate better-quality elements, which is essential for ensuring numerical stability and accuracy in finite element simulations. The finite element quality distributions for both spherical and cylindrical particles are illustrated in Figure 13. According to this figure, the great majority of tetrahedra feature quality between 0.3 and 0.8. This means that meshes generally show high quality, which is important for the accuracy of FEA results. Only a very small percentage of elements show a quality below 0.3, which can be explained considering that the quality threshold set for the automatic mesh generation algorithm is 0.2. This means that along automatic mesh generation and optimization, elements with a quality below 0.2 are eliminated and re-meshed to enhance mesh quality.

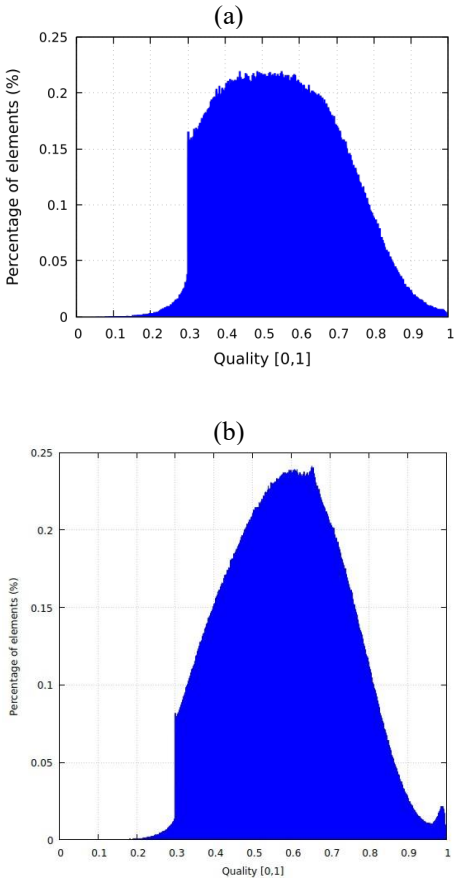

Figure 13. Mesh quality distribution: (a) spherical and (b) cylindrical particles.

To evaluate the apparent elasticity modulus (E_{app}), three types of boundary conditions are commonly employed: Kinematic Uniform Boundary Conditions (KUBC) and Static Uniform Boundary Conditions (SUBC), and Periodic Boundary Conditions (PBCs). It is well established that PBCs are advantageous in homogenization studies, as they lead to faster convergence of homogenized material properties while requiring smaller SVEs compared to KUBCs and SUBCs [6, 12, 35, 36]. However, applying PBCs is not just a boundary condition challenge but also a geometrical and meshing one. For PBCs to be effective, the particle generation process must be intrinsically periodic before meshing, and the mesh itself must maintain periodicity, ensuring that opposite faces have matching nodes to avoid interpolation errors when enforcing PBCs. While PBCs may be useful in some cases, Schneider et al. [37] highlight that achieving a fully periodic RVE and mesh topology is inefficient and challenging, especially for complex microstructures.

In this study, the primary objective is to achieve higher volume fractions without relying on the erosion of results method. This focus makes the direct enforcement of PBCs particularly difficult due to the lack of periodicity in the particle generation process and the disruption of mesh periodicity when applying a cutting plane. Unlike structured meshes, where node pairing is straightforward, the unstructured nature of the cut tetrahedral mesh complicates the identification of periodic node pairs and the imposition of displacement constraints.

Thus, to evaluate the apparent elasticity modulus (E_{app}), two types of boundary conditions are employed: KUBC and SUBC. Considering that mechanical properties of the glass-fiber composite are assumed to be isotropic, the macroscopically isotropic microstructure assumption is applied. Under this assumption, the apparent compressibility modulus (K_{app}), apparent shear modulus (G_{app}) and apparent elasticity modulus (E_{app}) are respectively calculated using equations (1), (2) and (3). In these equations, $\underline{\underline{\Sigma}}$ and $\underline{\underline{E}}$ are the volume averaged values (over the SVE) of stress and strain tensors obtained with FEA.

$$K_{app} = \frac{Tr\left(\underline{\underline{\Sigma}}\right)}{3Tr\left(\underline{\underline{E}}\right)} \tag{2}$$

$$G_{app} = \frac{1}{3}\left(\frac{\Sigma_{xy}}{2E_{xy}} + \frac{\Sigma_{yz}}{2E_{yz}} + \frac{\Sigma_{xz}}{2E_{xz}}\right) \tag{3}$$

$$E_{app} = \frac{9K_{app}G_{app}}{3K_{app} + G_{app}} \tag{4}$$

Using this FEA homogenization, the apparent elasticity modulus for KUBC and SUBC is calculated and presented in Table 10. These results are compared with the apparent elasticity modulus obtained using the erosion of results method described in section 2. A notable difference is observed between apparent elasticity moduli obtained with KUBC and SUBC when using the mesh cutting method, which is not the case when applying the erosion of results method. Moreover, the apparent elasticity modulus with KUBC and the mesh cutting method is higher than that obtained with KUBC and the erosion of results method. This is due to the fact that the erosion of FEA results from the SVE boundary tends to supress boundary condition effects. It is also observed that KUBC results tends to overestimate elastic properties by enforcing rigid displacements on the boundaries, while SUBC underestimates these

properties since it allows more boundary deformation. This difference highlights the contrasting effects of boundary conditions on the predicted material properties.

Table 10. Comparison of apparent elastic modulus with erosion of results method for KUBC and SUBC.

	Volume fraction with cut (%)	$E_{KUBC}\,(GPa)$	$E_{SUBC}\,(GPa)$	Volume fraction $_{\text{erosion of results}}$ (%) [26]	$E_{KUBC,\text{ erosion of results}}$ (GPa) [26]	$E_{SUBC,\text{erosion of results}}$ (GPa) [26]
Sphere	30.33 ± 0.49	7.41 ± 0.18	6.32 ± 0.06	34.12 ± 0.57	6.898 ± 0.096	6.906 ± 0.096
Cylinder	30.14 ± 0.53	8.45 ± 0.17	6.92 ± 0.11	27.01 ± 1.88	6.76 ± 0.29	6.64 ± 0.27

To validate results obtained, the evolution of apparent elasticity modulus with respect to the volume fraction of each SVE is also compared with analytical bounds of Reuss, Voigt and Hashin–Shtrikman (HS-, HS+) (Figure 14). It appears that, for each case, the apparent elastic modulus lies between lower and upper bounds, with a significant margin from Hashin–Shtrikman lower bound (HS-). This indicates that predicted apparent elastic moduli are neither overly conservative nor overly optimistic.

Figure 15 provides insights about how moving toward the core of the cube affects results. As the distance from boundary faces increases through the core of the SVE between 0 and of 0.2 (for a unit cube SVE) the change in volume fraction is not significant. This consistency confirms that the distribution of particles within the SVE is even and isotropic. In addition, as the distance from boundary faces increases, the differences between results obtained with KUBC and SUBC gradually diminish, which illustrates, as expected, that boundary conditions have very little effect at the core of the SVE. However, with the mesh cutting method, a clear difference between KUBC and SUBC results is observed, which demonstrates that the mesh cutting approach maintains the influence of boundary conditions.

(a)

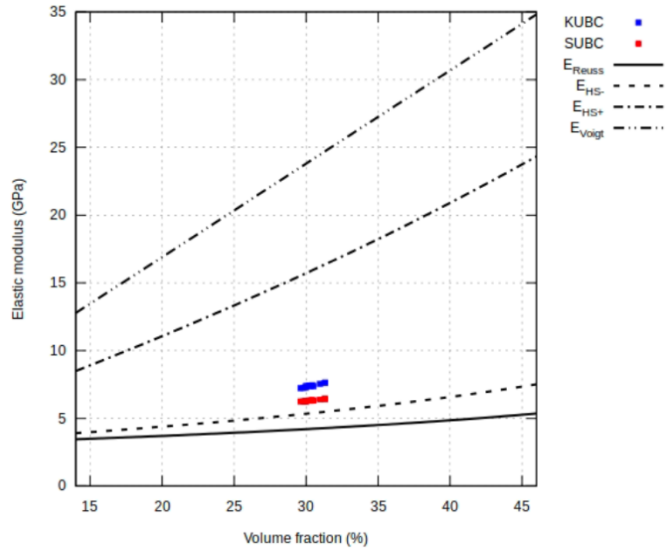

(b)

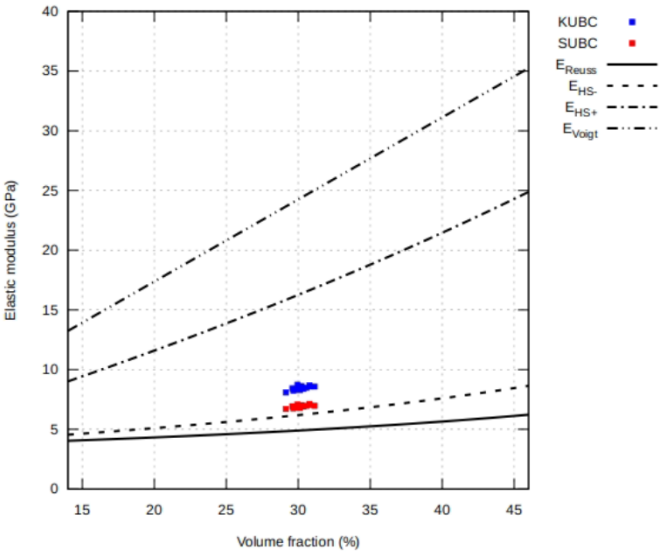

Figure 14. Elastic modulus scatter for different SVEs with: (a) spherical and (b) cylindrical particles.

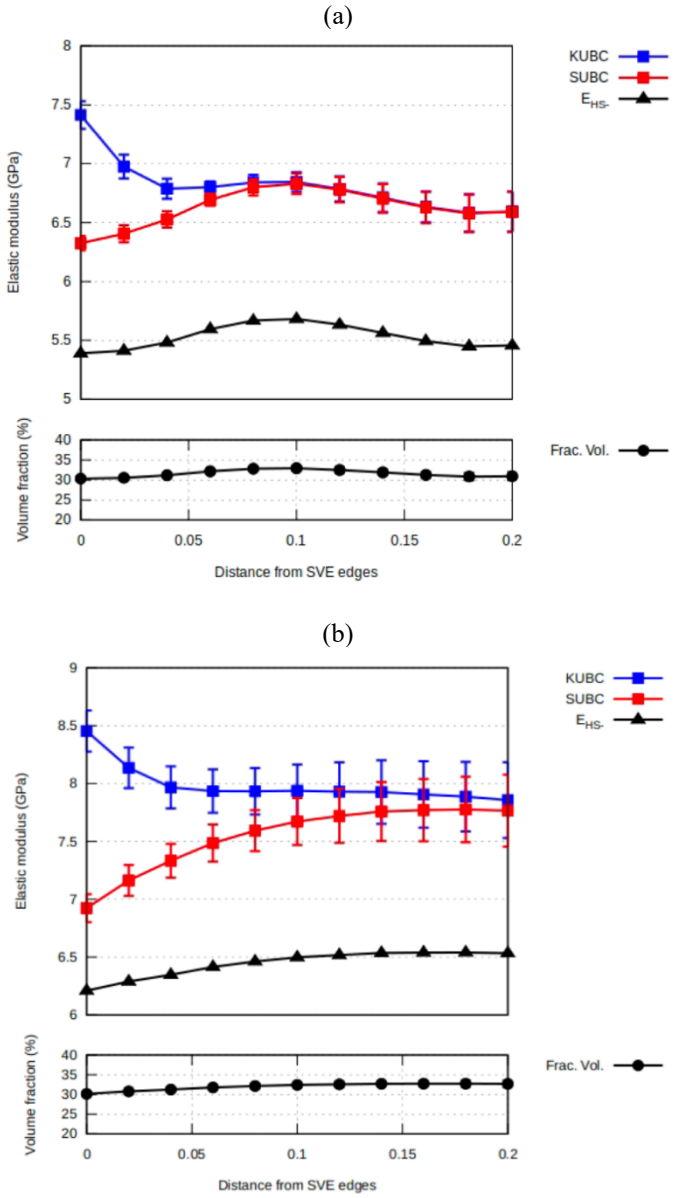

Figure 15. Elastic modulus scatter toward the core of the cube for a SVE with: (a) spherical and (b) cylindrical particles.

6. Conclusion

Modeling particle-based composites with high volume fractions continues to pose significant challenges. While considerable research has focused on achieving higher volume fractions, much of it has been limited to spherical

particles. The incorporation of cylindrical particles introduces additional challenges as they often come close to one another, which is consistent with reality. On the other hand, in computational models, limits are imposed on distances and angles between particles and between particles and boundaries of the SVE to ensure mesh convergence and avoid poorly shaped elements. To address the challenges associated with more complex shapes, such as elongated cylindrical particles, an automated approach for SVE generation is presented in this paper. This method leverages CAD-FEA integration through the UTM to automate all steps, from geometry generation to mesh creation, FEA, and, ultimately, numerical homogenization. However, applying the limits mentioned above (minimum distance and angle) leads to voids and a lack of particles near the SVE faces, resulting in lower volume fractions and non-uniform particle distribution. To tackle this issue of empty regions, FEA results in layers of elements from SVE faces can be excluded, which is referred to as the erosion of results method. The objective of this paper is to introduce adaptations to the automatic SVE generation process to avoid erosion of results. For this purpose, two methods are presented in this paper: the GCM, which slightly adjusts the size, location and orientation (for cylindrical particles) of particles to achieve a more efficient arrangement, and the mesh cutting method, which involves generating a larger domain, fully meshing its model and then cutting its mesh to attain the target SVE dimensions and volume fraction. This approach not only solves the problem of voids near the boundaries but also allows for comprehensive FEA on the entire final model, thereby enhancing the reliability of predicting mechanical properties in high-volume fraction composites. Both methods were separately applied to SVEs with spherical and cylindrical particles. The geometry modification method allows a limited increase (around 3%) of the volume fraction for both spherical and cylindrical particles, which justified a second approach. For the examples considered in this paper, the mesh cutting method increases the volume fraction by 11% for spherical particles and achieves a remarkable 14.8% increase for cylindrical particles, which allows reaching the target volume fraction more easily.

Future work will include a detailed comparison with experimental data to validate and refine the model, enhancing its predictive capabilities for practical applications. Future research also could focus on extending the application of these two methods to model high volume fractions of particles with large aspect ratios, such as more elongated particles, or even mixtures of particles with different shapes. Additionally, incorporating variability in particle properties, distributions, or the inherent complexity of real-world composite materials would provide a more comprehensive framework for simulating these systems. This would enable the evaluation of the effects of particle shape and aspect ratio on macroscopic material behavior. Exploring computational strategies to generate intrinsically

periodic microstructures before meshing, as well as developing post-processing techniques to restore periodicity after mesh modifications, are other aspects to consider. Furthermore, the potential of PBCs in achieving high volume fractions without erosion of results could be further investigated to assess its feasibility and benefits in this context.

References

[1] S. R. Mousavi *et al.*, "A review of recent progress in improving the fracture toughness of epoxy-based composites using carbonaceous nanofillers," *Polymer Composites,* vol. 43, no. 4, pp. 1871-1886, 2022.

[2] M. Y. Khalid, A. Al Rashid, Z. U. Arif, W. Ahmed, H. Arshad, and A. A. Zaidi, "Natural fiber reinforced composites: Sustainable materials for emerging applications," *Results in Engineering,* vol. 11, p. 100263, 2021.

[3] S. R. Mousavi *et al.*, "Mechanical properties of bamboo fiber-reinforced polymer composites: a review of recent case studies," *Journal of Materials Science,* vol. 57, no. 5, pp. 3143-3167, 2022.

[4] J. M. Ortolano González, J. A. Hernández Ortega, and X. Oliver Olivella, *A comparative study on homogenization strategies for multi-scale analysis of materials*. Centre Internacional de Mètodes Numèrics en Enginyeria (CIMNE), 2013.

[5] J. Ma, J. Zhang, L. Li, P. Wriggers, and S. Sahraee, "Random homogenization analysis for heterogeneous materials with full randomness and correlation in microstructure based on finite element method and Monte-carlo method," *Computational Mechanics,* vol. 54, pp. 1395-1414, 2014.

[6] K. Terada, M. Hori, T. Kyoya, and N. Kikuchi, "Simulation of the multi-scale convergence in computational homogenization approaches," *International Journal of Solids and Structures,* vol. 37, no. 16, pp. 2285-2311, 2000.

[7] I. Gitman, H. Askes, and L. Sluys, "Representative volume: Existence and size determination," *Engineering fracture mechanics,* vol. 74, no. 16, pp. 2518-2534, 2007.

[8] S. Mirkhalaf, F. A. Pires, and R. Simoes, "Determination of the size of the Representative Volume Element (RVE) for the simulation of heterogeneous polymers at finite strains," *Finite Elements in Analysis and Design,* vol. 119, pp. 30-44, 2016.

[9] W. J. Drugan and J. R. Willis, "A micromechanics-based nonlocal constitutive equation and estimates of representative volume element size for elastic composites," *Journal of the Mechanics and Physics of Solids,* vol. 44, no. 4, pp. 497-524, 1996.

[10] C. Huet, "Application of variational concepts to size effects in elastic heterogeneous bodies," *Journal of the Mechanics and Physics of Solids,* vol. 38, no. 6, pp. 813-841, 1990.

[11] S. Torquato and H. W. Haslach Jr, "Random heterogeneous materials: microstructure and macroscopic properties," *Appl. Mech. Rev.,* vol. 55, no. 4, pp. B62-B63, 2002.

[12] T. Kanit, S. Forest, I. Galliet, V. Mounoury, and D. Jeulin, "Determination of the size of the representative volume element for random composites: statistical and numerical approach," *International Journal of solids and structures,* vol. 40, no. 13-14, pp. 3647-3679, 2003.

[13] S. Nemat-Nasser and M. Hori, *Micromechanics: overall properties of heterogeneous materials*. Elsevier, 2013.

[14] A. Rasool and H. J. Böhm, "Effects of particle shape on the macroscopic and microscopic linear behaviors of particle reinforced composites," *International Journal of Engineering Science,* vol. 58, pp. 21-34, 2012.

[15] J. Segurado and J. Llorca, "A numerical approximation to the elastic properties of sphere-reinforced composites," *Journal of the Mechanics and Physics of Solids,* vol. 50, no. 10, pp. 2107-2121, 2002.

[16] A. El Moumen, T. Kanit, A. Imad, and H. El Minor, "Effect of reinforcement shape on physical properties and representative volume element of particles-reinforced composites: statistical and numerical approaches," *Mechanics of materials,* vol. 83, pp. 1-16, 2015.

[17] B. Widom, "Random sequential addition of hard spheres to a volume," *The Journal of Chemical Physics,* vol. 44, no. 10, pp. 3888-3894, 1966.

[18] J. Feder, "Random sequential adsorption," *Journal of Theoretical Biology,* vol. 87, no. 2, pp. 237-254, 1980.

[19] S. Kari, H. Berger, R. Rodriguez-Ramos, and U. Gabbert, "Computational evaluation of effective material properties of composites reinforced by randomly distributed spherical particles," *Composite structures,* vol. 77, no. 2, pp. 223-231, 2007.
[20] W. Tian, L. Qi, J. Zhou, J. Liang, and Y. Ma, "Representative volume element for composites reinforced by spatially randomly distributed discontinuous fibers and its applications," *Composite Structures,* vol. 131, pp. 366-373, 2015.
[21] A. Donev, S. Torquato, and F. H. Stillinger, "Neighbor list collision-driven molecular dynamics simulation for nonspherical hard particles. I. Algorithmic details," *Journal of computational physics,* vol. 202, no. 2, pp. 737-764, 2005.
[22] B. D. Lubachevsky, "How to simulate billiards and similar systems," *Journal of Computational Physics,* vol. 94, no. 2, pp. 255-283, 1991.
[23] B. D. Lubachevsky, F. H. Stillinger, and E. N. Pinson, "Disks vs. spheres: Contrasting properties of random packings," *Journal of Statistical Physics,* vol. 64, pp. 501-524, 1991.
[24] G. Li, F. Sharifpour, A. Bahmani, and J. Montesano, "A new approach to rapidly generate random periodic representative volume elements for microstructural assessment of high volume fraction composites," *Materials & Design,* vol. 150, pp. 124-138, 2018.
[25] W. Tian, X. Chao, M. Fu, and L. Qi, "An algorithm for generation of RVEs of composites with high particle volume fractions," *Composites Science and Technology,* vol. 207, p. 108714, 2021.
[26] A. Couture, V. François, J.-C. Cuillière, and P. Pilvin, "Automatic generation of statistical volume elements using multibody dynamics and an erosion-based homogenization method," *Computational Mechanics,* vol. 69, no. 4, pp. 1041-1066, 2022.
[27] A. Couture, V. François, J.-C. Cuillière, and P. Pilvin, "Automatic statistical volume element modeling based on the unified topology model," *International Journal of Solids and Structures,* vol. 191, pp. 26-41, 2020.
[28] S. Kari, H. Berger, and U. Gabbert, "Numerical evaluation of effective material properties of randomly distributed short cylindrical fibre composites," *Computational materials science,* vol. 39, no. 1, pp. 198-204, 2007.
[29] J.-C. Cuillière and V. Francois, "Integration of CAD, FEA and topology optimization through a unified topological model," *Computer-aided design and applications,* vol. 11, no. 5, pp. 493-508, 2014.
[30] C. P. Chrono. "An open source framework for the physicsbased simulation of dynamic systems." https://projectchrono.org/ (accessed.
[31] S. D. Porumbescu, B. Budge, L. Feng, and K. I. Joy, "Shell maps," *ACM Transactions on Graphics (TOG),* vol. 24, no. 3, pp. 626-633, 2005.
[32] K. Erleben, H. Dohlmann, and J. Sporring, "The adaptive thin shell tetrahedral mesh," 2005.
[33] P. Areias and T. Rabczuk, "Steiner-point free edge cutting of tetrahedral meshes with applications in fracture," *Finite Elements in Analysis and Design,* vol. 132, pp. 27-41, 2017.
[34] P. J. Frey and P.-L. George, "Mesh Generation: Application to Finite Elements." ISTE Ltd., 2008, ch. 19.
[35] F. Larsson, K. Runesson, S. Saroukhani, and R. Vafadari, "Computational homogenization based on a weak format of micro-periodicity for RVE-problems," *Computer methods in applied mechanics and engineering,* vol. 200, no. 1-4, pp. 11-26, 2011.
[36] W. Tian, L. Qi, X. Chao, J. Liang, and M. Fu, "Periodic boundary condition and its numerical implementation algorithm for the evaluation of effective mechanical properties of the composites with complicated micro-structures," *Composites Part B: Engineering,* vol. 162, pp. 1-10, 2019.
[37] K. Schneider, B. Klusemann, and S. Bargmann, "Fully periodic RVEs for technological relevant composites: not worth the effort!," *Journal of mechanics of materials and structures,* vol. 12, no. 4, pp. 471-484, 2017.